Engineered Science
DOI: https://dx.doi.org/10.30919/es1241

Enhanced Adsorption of Mercury and Methylene Blue Using Silver and Surface Modified Zeolite-NaX derived from Rice Husk

Saule Zharylkan,[1, 2,#] Shynggyskhan Sultakhan,[1,#] Madina Suleimenova,[1, 2] Seitkhan Azat,[2, 3] Yerbolat Sailaukhanuly,[3] Marat Tulepov[1] and Zhandos Tauanov[1, 2, 4,*]

Abstract

This study presents the synthesis of zeolite-NaX from rice husk using the hydrothermal method. The synthesized material exhibited the formation of zeolite-NaX as confirmed by X-ray diffraction (XRD) analysis. The substance was subjected to further modifications through the silver (Ag^0) nanoparticles and surfactant sodium dodecyl sulfate (SDS) to further investigate the adsorption properties of mercury and dyes in water. As a result of the ion exchange reaction and reduction by silver nanoparticles (AgNPs), the particle size was 15-16.4nm. Cationic methylene blue and mercury ion (Hg^{2+}) adsorption onto unmodified and modified zeolites was studied using a batch equilibration method. The sorbent modified with silver nanoparticles was investigated for its ability to purify water from mercury ions (Hg^{2+}), resulting in an increased sorption capacity from q_{max} = 136.9 to 285.7 mg g^{-1}. The possibility of removing dyes from an aqueous medium at a neutral pH was also studied. The sorption capacity increased from 9.21 to 13.48 mg g^{-1} when the SDS modified the sorbent. During 24 hours, preliminary results showed that the removal of mercury ions from the solution ranged from 27 to 76% and the removal of methylene blue from 18 to 87% of the initial concentration.

Keywords: Synthetic zeolite; Water treatment; Methylene blue; Mercury; Rice husk ash; Nanocomposite; Silver nanoparticles.
Received: 30 July 2024; Revised: 21 August 2024; Accepted: 31 August 2024.
Article type: Research article.

1. Introduction

Industrial enterprises seriously threaten the environment by dumping pollutants into reservoirs and wastewater. Dumping toxic waste from various industrial sectors causes serious damage to water resources, aquatic organisms, and ecosystems in general.[1,2] This causes close attention to environmental protection, especially wastewater treatment. Wastewater from the textile industry is considered the most polluted industry.[3] The textile industry uses a large amount of water, and a large amount of wastewater is generated at different times. Heavy metals and dyes can cause serious health problems at low concentrations in industrial wastewater. In the textile industry, dyes are used to color products. One classification divides dyes into direct, indirect, acidic, and basic dyes.[4] The basic dyes that are actually cationic are usually salt compounds, and methylene blue is one of the most significant types of these dyes. Due to their high thermal and optical strength, they remain in nature for a long time. Even a small concentration of coloring compounds present in water can be very harmful. Methylene blue MB is widely used in the dyeing industry and veterinary medicine as a dermatological and biological marker to control the growth of fungi and intestinal parasites. MB dye is considered toxic, causing skin and eye irritation, ingestion, breathing problems, and even cancer due to its toxic and mutagenic nature. It is also a non-biodegradable dye that persists in the environment for a long time.[5] After using the dye, 10-70% of the amount used ends up in the aquatic ecosystem in the form of wastewater. Since after dyeing, the concentration of dyes in textile liquids is estimated at 10-200 mg/l. However, discharge partially or untreated wastewater containing MB dyes from any of the above-mentioned industries can lead to serious health risks. Their presence in low concentrations in the range of 10-50 mg/l is considered a serious problem for the environment and public health.[6]

[1] *Faculty of Chemistry and Chemical Technology, Al-Farabi Kazakh National University, Almaty 050040, Kazakhstan.*
[2] *LLP "Scientific Production Technical Center "Zhalyn", Almaty 050012, Kazakhstan.*
[3] *Laboratory of Engineering Profile, Satbayev University, Almaty 050013, Kazakhstan.*
[4] *Ecology Research Institute, Khoja Akhmet Yassawi International Kazakh-Turkish University, Turkestan, 161200, Kazakhstan.*
[#] *These authors contributed to this work equally.*
* *Email:* tauanov.zhandos@kaznu.kz, zhtauanov@nu.edu.kz (Z. Tauanov)

Heavy metals are an extremely dangerous form of pollution because, accumulating in living organisms, they can cause ailments and disorders.[5-8] Chromium (Cr), lead (Pb), nickel (Ni), mercury (Hg), cobalt (Co), iron (Fe), cadmium (Cd), and manganese (Mn) are some of the heavy metals that contaminate surface waters due to various industrial activities. Mercury, which is present in nature in various physical states, is considered one of the most dangerous heavy metals. Most mercury is used in various industrial sectors, such as the manufacture of electronic devices and polymers, metallurgy, pharmaceuticals, oil and gas processing, and many others.[9,10] As these pollutants do not decompose in nature, controlling and regulating the amount of water is crucial, especially when the concentration of heavy metal ions exceeds the permissible limits is crucial. Several methods, such as precipitation, element filtration, flocculation, biodegradation, ion exchange, and adsorption, have been used to solve the problem of heavy metal pollution in wastewater.[11-14] Among these methods, adsorption has become the most preferred method due to its cost-effectiveness, simplicity, rapid and highly efficient removal, and excellent surface area.[15,16]

Great progress has been made in chemistry, nanotechnology, and materials science, leading to the creation of new adsorbents that are highly effective in adsorbing pollutants, cost-efficient, eco-friendly, and selective. Many materials, such as clay, zeolites, bio-carbon, carbon nanotubes, chitosan, and activated carbon, have been studied and used as adsorbents to effectively treat wastewater contaminated with heavy metals. Recently, researchers have shown significant interest in using nanocomposite materials as adsorbents.[17-20] Rice husks (RH) are numerous agricultural residues in rice-producing countries. Unfortunately, a significant portion of the husk produced during rice processing is either incinerated or discarded as waste, even though part of it is converted into a useful product such as raw materials and absorbent.[21-23] Open burning of rice husks is common in many developing and poor countries, causing environmental and health problems, so exploring ways to use resources is crucial. Silica can be obtained from rice husks using two alternatives: high-temperature pyrolysis to produce rice husk ash or solvent extraction to produce sodium silicate from rice husks. Silica derived from rice husks has been identified as an excellent raw material for producing silica nanoparticles.[24] These nanoparticles have a large surface area and nanometer size, making them desirable for numerous applications, such as adsorption materials, fillers in composite materials and others. The presence of natural silica in agricultural waste represents a promising alternative commercial precursor to silica. Agricultural waste, such as rice husks, sawdust and rapeseed stems, have been at the center of extensive research and have been successfully transformed into valuable end products.[23-26] To the best of our knowledge, none of the existing studies have reported using rice husk-derived silica (SiO_2) as an effective and sustained adsorbent for treatment.

This study aims to obtain synthetic zeolite from agricultural waste, such as ash from rice husks (RH) containing a large amount of silica. The silica content can be used as a zeolite resource to solve the problem by removing mercury ions (Hg^{2+}) and methylene blue (MB) from an aqueous solution.

The most important task in this work is the synthesis of an adsorbent with high adsorption capacity, selectivity, fast kinetics and the possibility of reuse. This work used rice husks of the Almaty region (Balkhash district, Bakanas village) to produce synthetic zeolite using alkaline hydrothermal treatment. Synthetic zeolite has been modified with silver nanoparticles (AgNPs) to increase the affinity for mercury nanoparticles and improve separation using ion exchange and co-deposition methods, followed by reduction in a porous structure. Modification of zeolite with sodium dodecyl sulfate (SDS) significantly improves its adsorption properties for methylene blue. The modified zeolite surface attracts the cationic dye due to electrostatic interactions and enhances sorption through hydrophobic interactions due to SDS hydrocarbon chains. This process makes it possible to effectively remove methylene blue from aqueous solutions, making it suitable for water purification systems. The materials were characterized using advanced methods for determining the zeolite phase, their surface morphology, and chemical composition.

2. Experimental section

2.1 The characteristics of the materials

Rice husk (RH) ash samples were taken from the Almaty region. All RH samples were used as a baseline. Before the experiment, the RH samples were washed with running water and distilled water and completely dried. NaOH (99.0%) Sigma-Aldrich (St. Louis, Missouri, USA), $NaAlO_2$ (99,0%), $AgNO_3$ (99,9%) are used for the ion exchange of silver and subsequent reduction to nanoparticles, $NaBH_4$ (98,0%) is needed to reduce silver ions into silver nanoparticles on the surface of nanocomposites. Sodium dodecyl sulfate (SDS) and methylene blue with a molecular formula of $C_{16}H_{18}ClN_3S.3H_2O$ (>98.5%)

2.2 Characterization

The mineralogical composition of the samples was analyzed by X-ray phase analysis (XRD) using the MPD XCEL-221 diffraction system at 30 kV and 10 mA, with CuKa radiation. The morphological characteristics of the zeolite surface were studied using scanning electron microscopy (SEM) using a scanning electron microscope, and elemental analysis was performed using an energy dispersion spectrometer Si (Li) (Joel JSM-6490 LA, Japan) connected to SEM. The size and structure of composites were studied using a high-resolution transmission electron microscope (TEM) (JEM2100 LaB6 HRTEM, JEOL, Japan) operating at 80 kV. The chemical composition of synthetic and modified Zeolite-AgNPs was studied by X-ray fluorescence (XRF) at (Rigaku NEX CG II, Japan). Measuring the concentration of mercury ions on the

mercury analyzer RA-915M (St. Petersburg, Russia) with a pyrolysis nozzle (PYRO-915+). Nitrogen adsorption at −196 °C using Autosorb-1 (Quantachrome, Hook, UK) performed the pore size distribution and specific surface area analysis. The pore size distribution was calculated using the BJH method, while the specific surface area was determined using the BET method. pH meter (Multiparameter Water Quality Meter 900-UK) UV–vis spectrophotometer (Peak instruments, C-7000UV).

2.3 Synthesis of Zeolite from rice husks

Rice husks (RH) were washed with running water several times, then rinsed with distilled water and dried in a drying oven at 100 °C temperature until completely dried. The dried RH was fired in a muffle furnace at 600 °C temperature for 4 hours. The resulting RHA was mixed and triturated with sodium hydroxide in a ratio of 1:2. The resulting mass was weighed and burned at 300 °C temperature for an hour in a muffle furnace. After an hour, the mass was weighed, and deionized water was added to a ratio of 1:5 and filtered. Sodium aluminate was added (calculated by weight of + NaOH) and autoclave at 90 °C temperature for 10 hours. The resulting synthetic zeolite was washed with distilled water to pH 7.[27] The schematic diagram for obtaining rice husk-derived zeolite is shown in Fig. 1.

2.4 Synthesis of zeolite nanocomposite by AgNPs

The freshly prepared zeolite is impregnated with silver nanoparticles (AgNPs) by an ion exchange and reduction reaction. A conventional ion exchange reaction is carried out by adding 20 ml of an aqueous $AgNO_3$ solution per 1 g of synthetic zeolite and allowed to soak for 12 hours. The reaction container is covered with aluminum foil and stored in a dark place to prevent the oxidation of silver ions. The ion exchange suspension is dried at 120 °C for 3 hours. The soaking procedure is repeated twice to obtain silver ion exchange zeolites containing about 2% by weight of AgNPs. The obtained ZRH-AgNPs burned for 3 hours at a temperature of 500 °C, then for 4 hours it was reduced by silver ions using $NaBH_4$ as a reducing agent, thus obtaining a nanocomposite with a load of AgNPs (ZRH-AgNPs).[28]

2.5 Modification of zeolite by SDS

Samples of 100 ml of SDS, 0.5%, 1%, 2%, and 3% solutions were prepared in conical flasks, and 0.5 g of Zeolite Na-X was added to each flask. The mixtures were stirred at 300 rpm in a 25 ◦C for 24 h. In this study, MB has positive sulfonate groups, negatively charged zeolite Na-X surfaces repel. Similarly, SDS-modified zeolites were used for MB adsorption since these surfactants are anionic chemicals and MB is a positively charged basic dye.[29] The plausible reaction mechanism for modifying zeolite with SDS is shown in Fig. 2.

2.6 Particle size calculation using the Scherrer's method

The Scherrer formula in crystallography and X-ray diffraction relates the size of small particles to the width of diffraction peaks. This formula is commonly used to determine the sizes of various nanoparticles. The general view of the Scherrer formula is as follows Eq. (1):

$$D = \frac{K\lambda}{\beta \cos\theta} \quad (1)$$

wherein D-indicates the crystallite size, K is the shape constant (K is equal to 0.9, for cubic crystal), wavelength (λ) of the Cu-radiation was 1.54056 Å for CuK radiation, β is the full width of the reflection at half of the maximum intensity, and the diffraction angle is θ.[30]

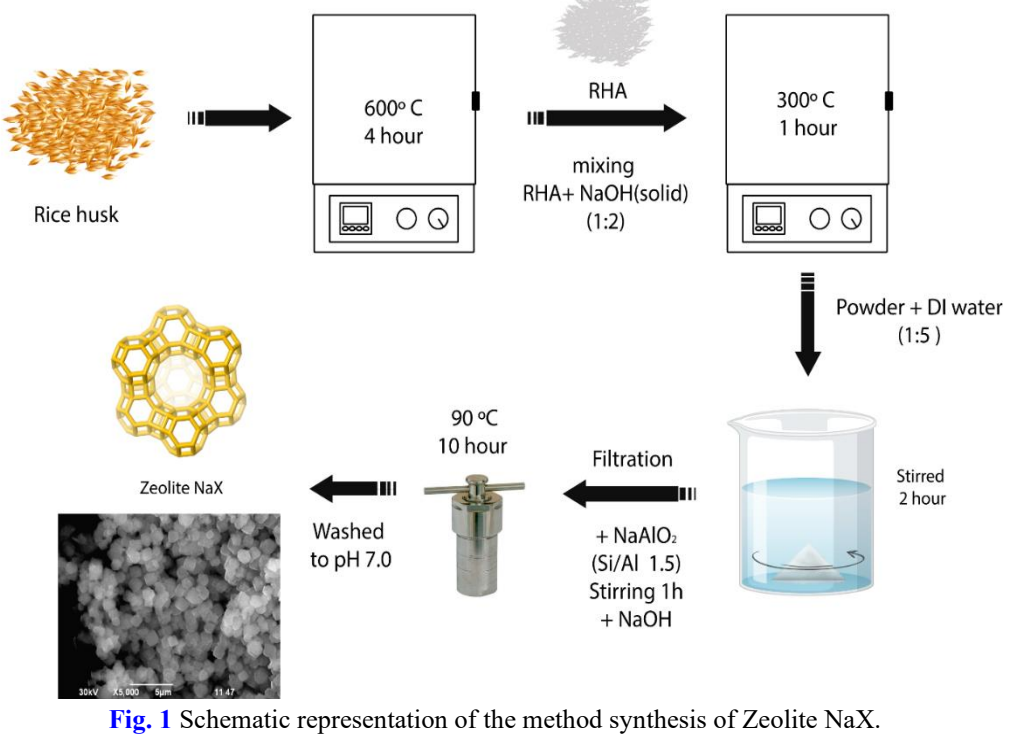

Fig. 1 Schematic representation of the method synthesis of Zeolite NaX.

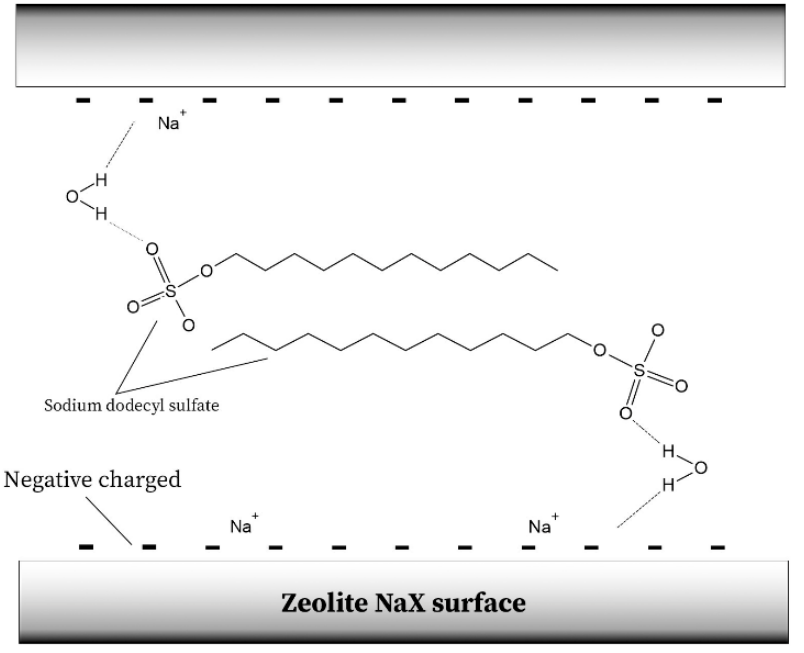

Fig. 2 The surface modification mechanism of zeolite with SDS.

2.7 Point zero charge

A sample of 0.2 g of each zeolite was added to 40.0 ml of 0.1 M NaCl in ten 50 ml plastic beakers. The pH was adjusted using a thermionic pH meter to 2, 3, 4, 5, 6, 7, 8, 9, 10, and 11 (± 0.1 pH unit) with 0.1 M HNO_3 and 0.1 m NaOH as needed for each container. They were then shaken for 24 hours on a rotator to achieve equilibrium. After this time, each pH value obtained was measured, and a graph of the initial pH value was plotted against the difference between the initial and final pH values.[31]

2.8 Batch adsorption isotherm for removal Hg^{2+} and methylene blue

The most used adsorption isotherm methods are the Freundlich and Langmuir models. This research method carried out a study of the maximum sorption capacity. Concentrations of 25, 50, 100, 150, 200, 300, and 400 mg l^{-1} were chosen as the initial sorption concentrations for methylene blue. A sample of 20 mg of pristine zeolite or composites was mixed with 10 ml of Hg^{2+} and MB solution at different initial concentrations from 10 to 500 mg l^{-1} in 15 ml plastic tubes. The quantity of the adsorbing substances was calculated by (Eq. (2)):

$$q_{max} = \frac{(C_i - C_{eq})\cdot V}{m}, \quad (2)$$

wherein q_{max} (mg g^{-1}) is the maximum adsorption capacity (mg g^{-1}), C_i, C_{eq} – the initial and equilibrium substances concentrations (mg l^{-1}), V –solution volume (l), m – the total mass (g) of adsorbent.

Langmuir and Freundlich isotherm models are used to evaluate experimental data to study adsorption behaviors. Langmuir isotherms have a linearized form and are expressed by Eq. (3)[32]

$$\frac{Ce}{q_{eq}} = \frac{1}{q_{max}\cdot K_L} + \frac{C_{eq}}{q_{max}}, \quad (3)$$

wherein Ceq (mg l^{-1}) is the equilibrium concentration of adsorbate; q_{eq}, q_{max} (mg g^{-1}) are the equilibrium and maximum sorption capacity; K_L (l mg^{-1}) is the Langmuir constant.

The linear form of the Freundlich isotherm is expressed in Eq. (4)[32]:

$$\log_{eq} = \log K_F + \frac{1}{n}\log C_{eq}, \quad (4)$$

wherein Ceq (mg l-1), q_{eq} (mg g^{-1}) are the equilibrium concentrations of adsorption capacity, while n (dimensionless) and K_F are Freundlich constant.

The Temkin model is explained with the following Eq. (5)[32]:

$$q_e = A + B \ln C_e \quad (5)$$

In the mentioned model,s, A and B are signified as isotherm constants.

The Dubinin-Radushkevich model is expressed as the following Eq. (6)[32]:

$$\ln q_e = \ln q_m - K\varepsilon^2 \quad (6)$$

where K indicates the adsorption energy constant, and ε is the Polanyi potential, calculated from Eq. (7)

$$\varepsilon = RT \ln\left(1 + \frac{1}{C_e}\right) \quad (7)$$

The mean free energy of adsorption, E (kJ/mol), was calculated using Eq. (8).

$$E = \frac{1}{\sqrt{2K}} \quad (8)$$

2.9 Batch adsorption kinetics for the removal of Hg^{2+} and methylene blue

Adsorption kinetics were studied using 40 ml of a freshly prepared aqueous solution of Hg^{2+} with an initial concentration of 100 mg l^{-1} and an adsorbent dosage of 0.1 g.

Concentrated nitric acid was used to adjust the pH of a solution to 2.5, which allowed the precipitation and hindering effects of mercury complexes to be avoided. The details of speciation studies using Medusa software and the possible formation of mercury complexes under certain conditions can be found elsewhere. The experiments were carried out at an ambient temperature and static conditions. Each kinetics point (0.5 - 24 h) was analyzed using 15 µL of aliquot from adsorption containers. Additional information about speciation studies conducted using the Medusa software and the possibility of mercury complexes under certain conditions can be found in other sources.[33]

The adsorption capacity of the dye was evaluated by placing the adsorbent in aqueous solutions of the dye and shaking at a speed of 150 rpm. The MB solution was prepared at a concentration of 100 (mg l^{-1}) before the adsorption test and diluted to the desired concentrations required for experiments. Contact time (1-24 h) adsorbent dose 0.1 g. The concentration of MB at the beginning and equilibrium state was measured at a maximum wavelength (λ_{max}) of 665 nm using a UV–vis spectrophotometer using the standard curve method. The standard curve for the analysis of MB concentration and maximum absorption wavelength is shown in the S1. The exploration of adsorption kinetics was carried out using three models: pseudo-first-order (PFO), pseudo-second-order (PSO), and intraparticle diffusion (IPD) models, represented by the following equations:[32]

$$\log(q_e - q_t) = \log q_e \frac{K_1}{2.303} t \quad (9)$$

$$\frac{t}{q_t} = \frac{1}{k_2 q_e^2} + \frac{t}{q_e} \quad (10)$$

$$q_t = K_d t^{0.5} + C \quad (11)$$

In this equation, K_1 (min^{-1}) and k_2 (g/mg min) are the emblems of the rate constant.

The percentage of deletion is calculated using the formula:

$$R(\%) = \frac{C_i - C_e}{C_i} \times 100 \quad (12)$$

2.10 Error analysis

The optimal isotherm model is determined by the correlation coefficient (R^2) analysis. Although this method is useful for evaluating the effectiveness of correlation analysis, it has limitations when working with inherently nonlinear isotherms. Therefore, three error functions are used to select the most appropriate model reflecting experimental data.[34] These functions are presented as Eq. (13-15).

The sum of Squared Errors $SSE = \sum_{i=1}^{n}(q_{e,cal} - q_{e,meas})^2$ (13)

The sum of absolute errors $SAE = \sum_{i=1}^{n}(q_{e,cal} - q_{e,meas})_i$ (14)

Average relative error $ARE = \frac{100}{n}\sum_{i=1}^{n}(\frac{q_{e,cal} - q_{e,meas}}{q_{e,meas}})_i$ (15)

3. Results and discussion

3.1 Characterization

Synthetic zeolites and nanocomposites obtained from rice husk ash were examined using an XRD to determine the mineralogical phase and confirm the crystal structure. According to the results, the obtained synthetic zeolite and nanocomposite were confirmed by characteristic peaks of the AgNPs phases at 38.2° and 44.2° in the matrix, as shown in Fig. 3. Additionally, the size of silver nanoparticles (AgNPs) was analyzed from the XRD analysis results using the Scherrer equation method and the calculated size is D=16,4 nm.

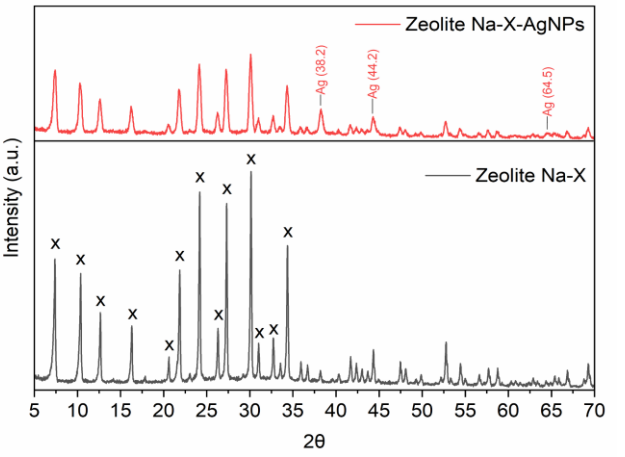

Fig. 3 XRD of Zeolite Na-X - AgNPs, Zeolite Na-X.

The SEM-EDX results of the obtained zeolites are shown in Fig. 4A. The SEM image shows that the zeolite particles are agglomerates. Upon magnification, each zeolite-NaX particle has a regular cubic shape, which is evidence that the synthesized material has a good structural shape. The elemental analysis results by the EDS method (Table 1) showed the silver nanoparticles' successful modification of the zeolite. The average percentage of silver nanoparticles in the structure of synthetic zeolite after the co-deposition reaction was (2.05 ± 0.05 %) for the composite, the composite has an atomic ratio of Al:Si = 1:1. In the SEM images (Fig. 4A), it is clear that when modifying the zeolite with silver, it does not affect its integrity, which can be seen from the SEM photograph of Zeolite-NaX Ag NPs, this indicates that when modified with silver, it occurs only on the surface of the particles. The presence of Ag nanoparticles and the range of particle distribution were also analyzed on micrographs by the TEM method and the results are shown in Fig. 4B. The results show that the nanoparticles are relatively uniformly distributed in a synthetic zeolite matrix with an average nanoparticle size of 15 nm.

The elemental composition of the synthetic zeolite and nanocomposite is shown in Table 2. The content of all elements is presented in %. According to the results, the Zeolite NaX-AgNPs content of Ag in the structure is 0,5950%. The results of the BET surface analysis show that the actual surface area of Zeolite NaX, Zeolite NaX-AgNPs and Zeolite NaX-SDS is increasing. Synthetic zeolite NaX showed a surface area of 6.25 m^2 g^{-1}, and nanocomposite showed 6.6 m^2 g^{-1} and 8.389 m^2 g^{-1}, respectively. When modifying synthetic zeolites with particles, there was no significant change in the

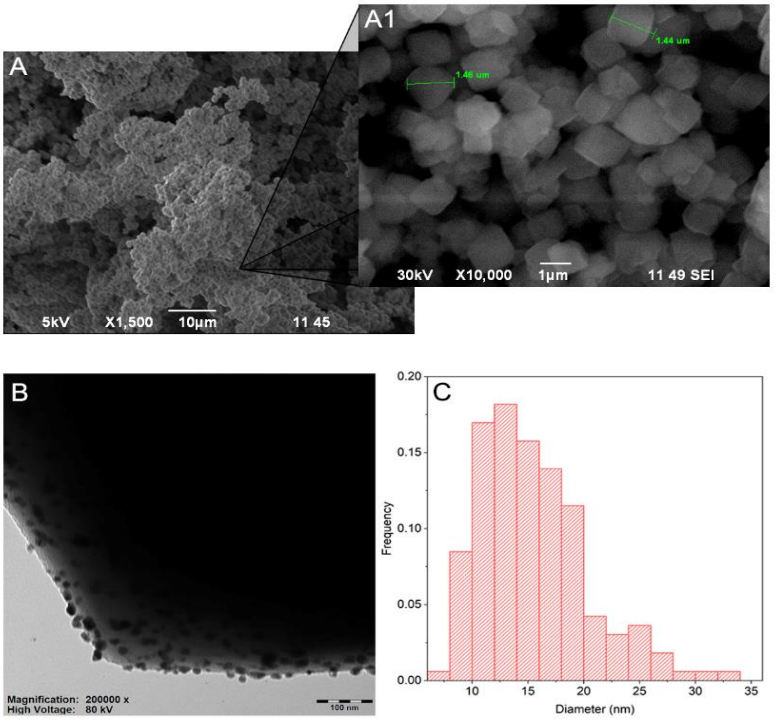

Fig. 4 Synthetic zeolites (A-A1) – microimages of SEM, A-1500x. A1-10000x. (B) - TEM image of zeolite AgNPs sample, (C) – histogram of the propagation frequency of silver nanoparticles on the surface of zeolite AgNPs sample in TEM image.

Table 1. Result of EDS analysis of Zeolite Na-X and Zeolite Na-X AgNPs.

Substance	Mass, %					
	C	O	Na	Al	Si	Ag
Zeolite NaX	16.34 ±0.43	47.38 ±0.72	10.49 ±0.34	13.34 ±0.38	12.45 ±0.39	-
Zeolite NaX-AgNPs	5.70 ±0.08	47.55 ±0.16	13.80 ±0.09	15.24 ±0.08	15.52 ±0.09	2.05 ±0.05

Table 2. Result of XRF analysis of Zeolite Na-X and Zeolite Na-X AgNPs.

Substance	Mass, %			
	Al_2O_3	SiO_2	Na_2O	Ag
Zeolite Na-X	36.9	63.1	ND	0.0007
Zeolite Na-X AgNPs	36.7	62.6	ND	0.5950

Table 3. The porosimetric analysis of the Zeolite NaX, Zeolite NaX-AgNPs and Zeolite NaX-SDS.

Sample name	BET Surface area (m^2 g^{-1})	Pore size (nm)	Total Pore Volume (cm^3 g^{-1})	Micropore Volume (cm^3 g^{-1})
Zeolite NaX	6.250	0.9462	0.0035	0.0026
Zeolite NaX-AgNPs	6.600	1.0176	0.0026	0.0016
Zeolite NaX-SDS	8.389	-	-	-

surface area, which could be due to partial blockage of micro- and mesopores. As shown in Table 3, the pore sizes of Zeolite NaX and Zeolite NaX-AgNPs showed about 1 nm.

Zeolite-NaX and Zeolite NaX-SDS (2%) SDS has a distinctive fingerprint at 3235-3380 cm^{-1} indicating the presence of hydroxyl groups of water. The single compound of SDS has a symmetric stretching vibration of SO_2 molecule at 1080 cm^{-1} at 950-1100 cm^{-1}, which shows the S = O stretching vibration. J.A. Raj and others[35-40] have also reported that the two bands at 1030 and 1000 cm^{-1} became visible due to SO_3^- molecular stretching indicating the presence of anionic surfactant molecules in polyaniline. Meanwhile, the peaks at 2919, 2919, and 2851 cm^{-1} correspond to CH_2 stretching and bending modes. These are characteristics of a polar environment. The 1227 cm^{-1} peak corresponds to skeletal vibration involving the bridge S–O stretch, while the 1077 cm^{-1} peak corresponds to the C–C band stretching. The 827 and 579 cm^{-1} peaks correspond to asymmetric C–H bending of the CH_2 group.

The peak at 3426 cm^{-1} is in the range of 3300-3500 cm^{-1}, which is typical for stretching vibrations of the amino group (-NH). It indicates the presence of amino groups in the molecule of methylene blue. 1600 cm^{-1}: This peak is situated in the region of 1500-1600 cm^{-1}, corresponding to the aromatic

vibrations of benzene rings. Methylene blue contains two benzene rings, and this peak is associated with the vibrations of aromatic bonds within these rings. 1534 cm^{-1}: A peak in this region may also be associated with aromatic vibrations, possibly providing additional details regarding the structure of benzene rings or adjacent functional groups. 1341 cm^{-1}, 1366 cm^{-1}: This peak may be related to vibrations of alkyl groups, possibly including vibrations of the methylene bridge (-CH_2-). Such vibrations are commonly observed in this spectral region. In the presented work, pH metric measurements were carried out to determine whether SDS on the surface of synthetic Zeolite NaX changes the surface charge of the adsorbent by determining the point zero charge. The results are shown in Fig. 5. The surface charge characteristics of adsorbents at different pH values affect the adsorption capacity in the solution adsorption system. The experimental pHpzc value of synthetic zeolite was 7.51, and after modification, it was 7.96. The surface charge is positive at pH 7>pH_{pzc} and negative at pH 7<$pH_{pzc.}$ This indicates the surface charge of adsorbents is negative. With an increase in the negative charge of the adsorbent surface due to deprotonation of the carboxyl group, the electrostatic attraction between MB increased, thereby increasing the adsorption capacity of Zeolite NaX-SDS.

These data imply that at any pH lower than 4.5, where most mercury is removed from the solution, both materials have a positive surface charge that should repeal positively charged Hg^{2+} cations. However, an overlooked aspect in the related literature is the speciation of ions in solutions, especially in complexing agents such as Cl^- ions. The speciation of the system studied is presented in Fig. 6. Evidently, at pH < 4.5, the predominant species is a neutral soluble $HgCl_2$. Thus, the surface charge is not expected to affect the uptake of Hg species under these conditions.

3.2 Adsorption kinetics

Preliminary results of the adsorption kinetics show a significantly higher mercury removal from the solution than the initial zeolite, as shown in Fig. 7. The lowest values of the zeolite, which showed adsorption removal, are only 27.3% after 24 hours. The modified silver nanoparticles showed markedly improved removal efficiency. The residual concentrations of mercury ions in water during the first hour of adsorption showed that the removal efficiency was 43.4%. After 24-hour adsorption kinetics of Zeolite NaX-AgNPs, 76.8 % of mercury ions were removed, which is 1.7 times higher than when removing the original synthetic zeolite. The effect of contact time on the sorption of MB for adsorbent and an initial concentration of 10 ppm at different times is shown in Fig. 7. The results show that the initial zeolite removal efficiency was 19% and the zeolite showed 87.7%. With an increase in the time of technological contact, adsorption will increase due to an increase in the contact of dye molecules with Zeolite NaX-SDS. An increase in adsorption occurs due to an increase in contact time until an equilibrium value of about 24 hours is reached. As can be seen, the dye molecules are initially adsorbed at a high rate, which then gradually decreases until the adsorption on the adsorbent reaches equilibrium. Moreover, the parameters of the models are presented in Table 4. The highest value of R^2 (0.98-0.99) was obtained for a pseudo-second-order kinetic model for all samples. In addition, the qe value calculated using this model is closest to the experimental qe values. Therefore, it can be concluded that the adsorption of MB dye and Hg^{2+} on Zeolite NaX-AgNPs and Zeolite NaX-SDS is most accurately described by the pseudo-second model. Thus, it can be concluded that the adsorption of MB dye and Hg^{2+} is not limited only to chemical adsorption but is also carried out under the combined influence of chemical adsorption, physical adsorption, and adsorption on the inner surface.

In modeling the sorption kinetics using the Interparticle Diffusion model, the sorption process for all adsorbents can be roughly divided into two stages. For Zeolite NaX – MB, the first stage (0-2 hours) shows a Kd value of 0.083, indicating slow diffusion of the adsorbate between the adsorbent particles, which may suggest a higher degree of hindered transport or a denser adsorbent structure. This Kd value decreases to0.035 in the subsequent stage. For Zeolite NaX-SDS – MB, the first stage (0-6 hours) has a Kd value of 0.582, indicating faster

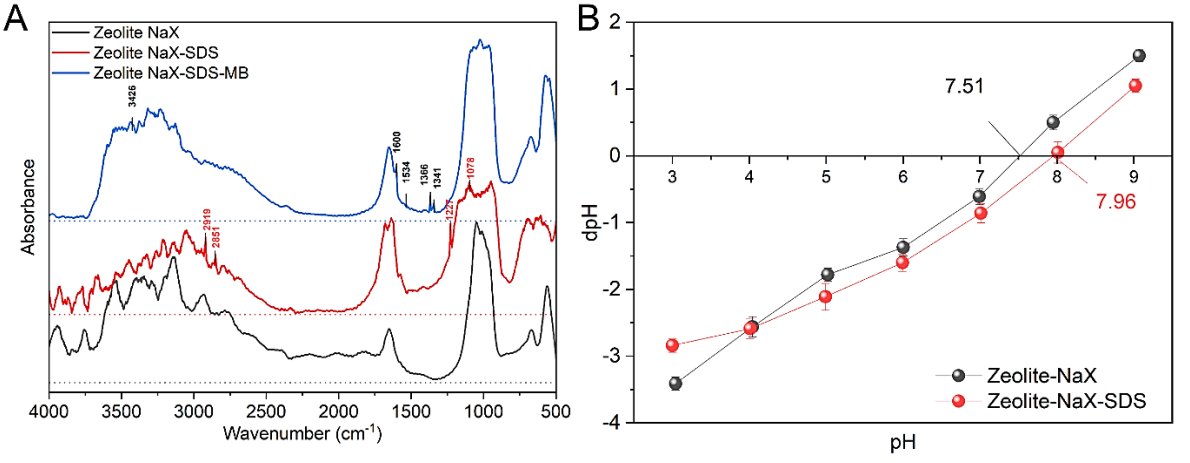

Fig. 5 (A) FT-IR of Zeolite Na-X, Zeolite Na-X - SDS, Zeolite Na-X – SDS-MB; (B) Plot of Δ(pH) vs. pH measured for Zeolite Na-X and Zeolite Na-X – SDS.

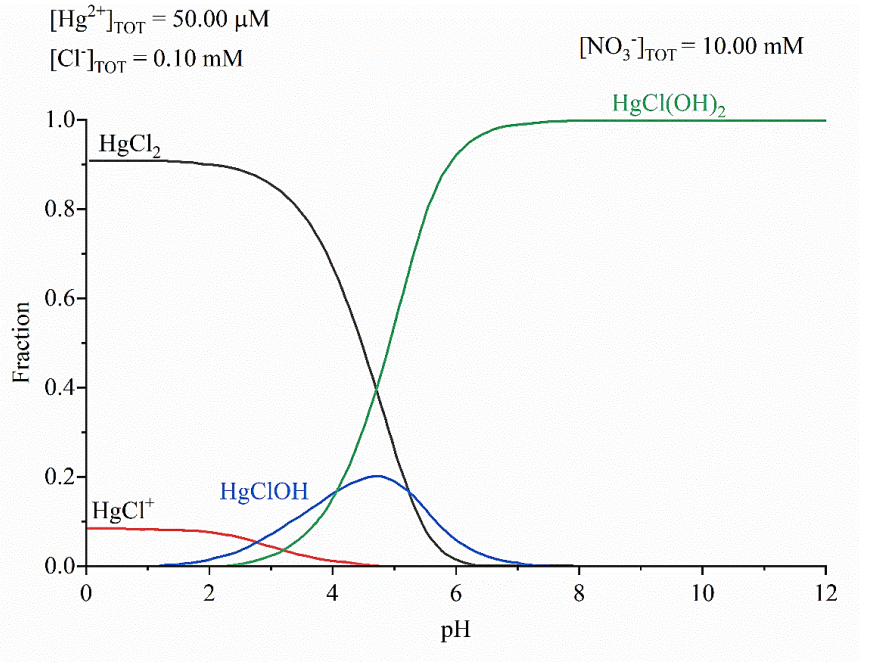

Fig. 6 Speciation of 10 mg cm-3 Hg^{2+} solution (0.05 mmol Hg^{2+}, 0.1 mmol Cl^{-}) [Diagram created by Medusa software].

Table 4. Parameters of adsorption kinetics for the removal of Hg^{2+} and MB.

Model	Parameter	MB		Hg^{2+}	
		Zeolite NaX	Zeolite NaX-SDS	Zeolite NaX	Zeolite NaX-AgNPs
PFO	q_e,mg g^{-1}	1.73	4.63	2.47	9.78
	K_1	0.001	0.003	0.024	0.003
	R^2	0.961	0.990	0.939	0.950
	SAE	0.56	1.96	1.04	3.71
	SSE	0.08	0.91	0.27	2.95
	ARE	0.31	-3.83	0.96	-0.40
PSO	q_e mg g^{-1}	2.7	7.9	5.6	15.7
	K_2	0.17	5.06	2.79	42.78
	R^2	0.993	0.999	0.988	0.988
	SAE	0.74	1.64	1.47	1.43
	SSE	0.13	0.83	0.55	0.61
	ARE	0.83	-3.57	0.88	-1.62
IPD			Stage 1		
	K_d	0.083	0.582	0.151	0.165
	C	0.414	0.882	1.798	7.118
	R^2	0.999	0.927	0.906	0.947
			Stage 2		
	K_d	0.035	0.169	0.191	0.152
	C	1.173	2.905	1.150	9.387
	R^2	0.992	0.998	0.972	0.995

diffusion of the adsorbate, which may reflect the positive impact of SDS on the sorption process. This value then decreases to 0.169 in the second stage. For Zeolite NaX – Hg2+, the first stage (0-6 hours) has a Kd value of 0.151, and in the second stage, it increases to 0.191. The increase in Kd in the second stage may indicate more efficient diffusion, possibly related to changes in the adsorbent structure or dynamic changes during the sorption process. For Zeolite NaX-AgNPs, the Kd value in the first stage (0-4 hours) is 0.165, and in the second stage, it is 0.152. The small changes in Kd values suggest that the diffusion process gradually stabilizes, and the dynamics become less pronounced as the sorption process nears completion.

3.3 Adsorption Isotherm

The Langmuir, Freundlich, Temkin and Dubinin-Radushkevich (D-R) models were used to determine the adsorption performance of materials (Table 5). The periodic

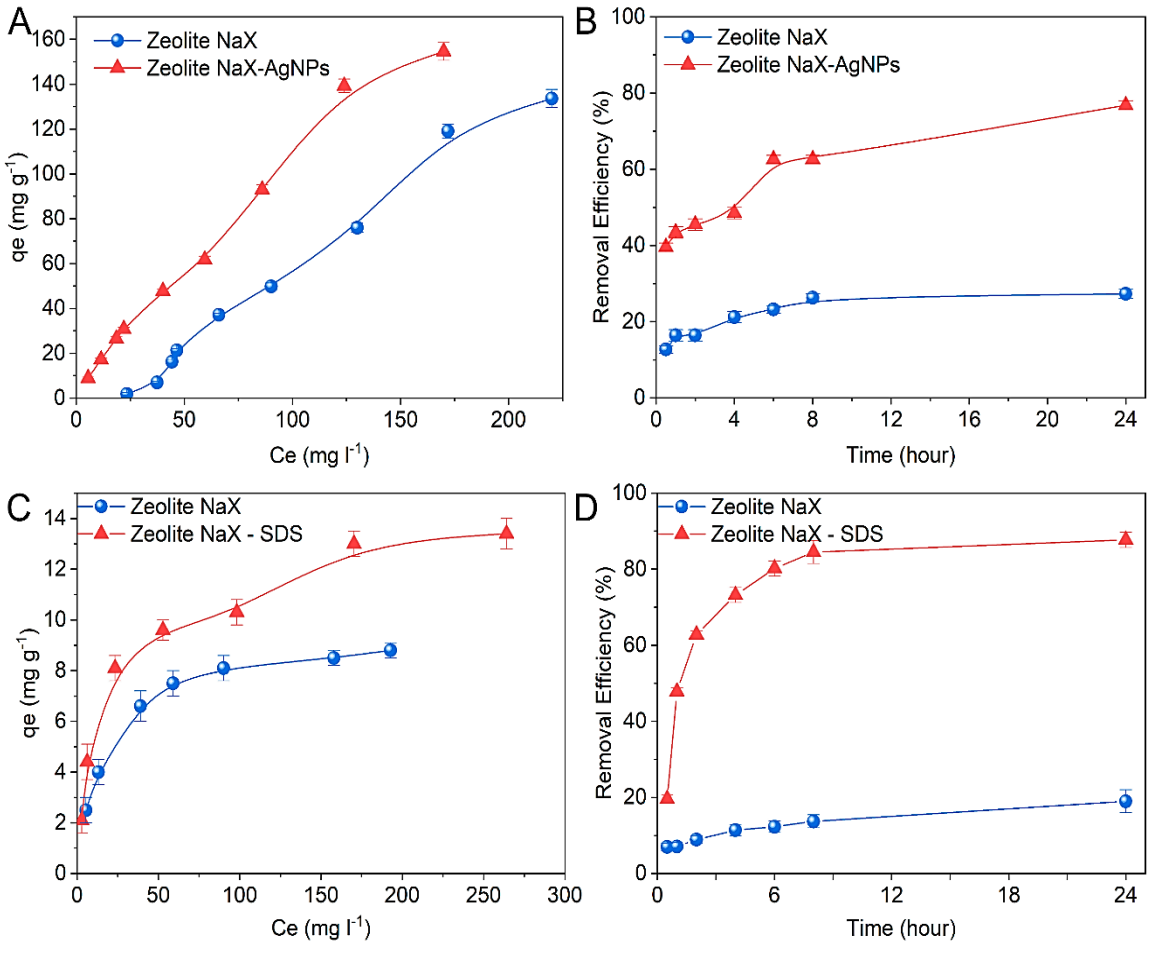

Fig. 7 The adsorption kinetics and isotherms of Zeolite NaX, Zeolite NaX-SDS and Zeolite NaX-AgNPs for the removal of MB(A, B) and Hg^{2+}(C, D).

adsorption isotherm was studied to study the adsorption characteristics of the initial and modified zeolite. According to the results of the Langmuir model, the initial synthetic zeolite demonstrated the adsorption capacity of q_{max} = 9.2 mg g^{-1} to remove MB from water, which is due to physical adsorption, since it was found that the zero-charge surface of the zeolite surface is negatively charged. When modifying the zeolite surface, a more negative charge occurs, thereby increasing the sorption characteristic of the zeolite to q_{max}=13.48 mg g^{-1}. The maximum adsorption capacity of synthetic Zeolite NaX is about 136,98 mg g^{-1}; after modification by silver nanoparticles, Zeolite NaX-AgNPs increased by two times to 285,71 mg g^{-1} to remove mercury ions. The results show that the silver-containing composite has a much higher adsorption capacity than synthetic zeolite.

According to the Temkin model for the sorption of mercury ions, the B value for Zeolite NaX is 29 J mol^{-1}, indicating that as the adsorbent's surface coverage increases, the interaction between the adsorbate molecules and the surface weakens. For Zeolite NaX-AgNPs, the B value is 35 J mol^{-1}, suggesting that the adsorption energy decreases more significantly as the surface coverage by the adsorbate increases. A higher B value indicates that the heat of adsorption decreases more rapidly, which may be due to the initial surface sites having higher interaction energies, while the available sites have lower energies as the surface coverage increases. This could indicate the heterogeneity of the adsorbent surface or strong interactions during the initial stages of adsorption, which weaken as the surface coverage increases. According to the Dubinin-Radushkevich model, the E value for Zeolite NaX is 37.06 kJ/mol, indicating moderately strong interactions between the adsorbate and the adsorbent, which may be associated with both physical and initial stages of chemical adsorption. For Zeolite NaX-AgNPs, the E value is 132.55 kJ/mol, suggesting very strong chemical interactions, implying robust chemical bonds or specific physicochemical interactions. This value indicates high adsorption strength and difficult desorption.

Following the coefficient of determination R^2 values, it seems that the Langmuir model R^2 = (0.98-0.99) provides a more accurate representation of experimental observations. MB dye and Hg^{2+} were absorbed on the surface of adsorbents compared with the Freundlich model R^2 = (0.91-0.97), and the adsorption of MB dye and Hg^{2+} molecules was carried out in a monolayer mode. In addition, it was calculated that the maximum adsorption of Hg^{2+} and MB nanocomposite (Zeolite NaX-AgNPs) and zeolite-SDS was 285.71 mg g^{-1} and 13.48 mg g^{-1}, which is higher than that of the previously described

Table 5. Suitable parameters of the isothermal adsorption line for the removal of Hg^{2+} and MB.

Model	Parameter	MB		Hg^{2+}	
		Zeolite NaX	Zeolite NaX-SDS	Zeolite NaX	Zeolite NaX-AgNPs
Langmuir	q_{max}, mg g^{-1}	9.21	13.48	136.98	285.71
	K_L, l mg^{-1}	0.067	0.067	0.0046	0.0058
	R^2	0.9998	0.9909	0.9802	0.9981
	SAE	1.05	6.45	4.30	4.51
	SSE	0.23	7.61	3.59	4.39
	ARE	-0.38	-0.31	0.61	1.01
Freundlich	n, mg g^{-1}	0.341	0.378	0.994	1.019
	kF	1.657	1.947	0.542	1.177
	R^2	0.9249	0.9215	0.9791	0.917
	SAE	4.86	10.10	7.60	11.20
	SSE	4.29	18.81	14.44	19.78
	ARE	0.64	-1.97	-2.39	7.70
Temkin	A	0.797	0.887	0.045	0.105
	B, J mol^{-1}	1.826	2.532	29.258	35.894
	R^2	0.9756	0.9952	0.9915	0.9768
	SAE	2.33	1.60	7.01	7.68
	SSE	0.86	0.49	14.33	22.27
	ARE	0.90	1.23	10.72	-0.99
D-R	q_m, mg g^{-1}	8.28	12.88	74.09	160.68
	E, KJ mol^{-1}	52.14	57.33	37.06	132.55
	R^2	0.9600	0.7373	0.8213	0.8701
	SAE	1.94	9.10	12.78	13.60
	SSE	0.98	34.12	73.87	63.94
	ARE	0.12	-11.96	4.00	10.25

Table 6. MB and Hg^{2+} adsorption of various adsorbents.

Adsorbent	Adsorbate	Adsorption capacity, mg g-1	References
Dithizone/Natural zeolite	Hg^{2+}	2.62	[36]
NaP-zeolite	Hg^{2+}	103.2	[37]
Natural zeolite	MB	10.78	[38]
Unmodified zeolite/ 2% SDBS-modified zeolite	MB	8.7 / 15.7	[39]
Unmodified natural zeolite/ Magnetic zeolite	MB	7.7 / 9.6	[40]
Synthetic Zeolite NaX/ Synthetic Zeolite NaX modified AgNPs	Hg^{2+}	136.88 / 285,71	This work
Synthetic Zeolite NaX/ Synthetic Zeolite NaX modified SDS	MB	9.21 / 13.48	This work

zeolite-based adsorbents (Table 6). This result suggests that nanocomposite and Zeolite NaX-SDS may serve as an efficient and low-cost adsorbent for Hg^{2+} and MB.

According to Inglezakis *et al.*[41] and Tauanov *et al.*[42], mercury ions in solution react with metallic silver (Ag^0) at a theoretical stoichiometric ratio of Hg/Ag equal to 0.5, which leads to the formation of zero-valent mercury:

$2Ag^0 + Hg^{2+} \rightarrow 2Ag^+ + Hg^0$

$0.9Hg^0 + 1.1Ag^0 \rightarrow Ag_{1.1}Hg_{0.9}$

$3Hg^0 + 2Ag^0 \rightarrow Ag_2Hg_3$

A higher molar ratio of Hg: Ag in the reduction of Hg^{2+}, compared with the reduction of Hg^0, leads to higher removal efficiency. Therefore, the nanocomposite Zeolite-NaX-AgNPs demonstrated substantial improvement compared to pristine zeolite. However, this is only part of the overall mechanism as other reactions, including amalgamation follow redox.

4. Conclusions

In conclusion, this research paper presented the successful synthesis of zeolite NaX by hydrothermal method from SiO_2, which was obtained from rice husks by burning it. The obtained material was also confirmed through XRD and XRF analyses. The BET result determined that the resulting material has equally micropores and mesopores; the average pore diameter is 1 nm, and the average pore diameter determined by the BJH method is 29.7 nm. The synthesized

material and its modified derivatives were tested for their sorption characteristics of Hg^{2+} ions and methylene blue dye using the Langmuir, Freundlich, Temkin, and Dubinin-Radushkevich models. The study found that the starting material has a sorption capacity of 9.21 mg g^{-1} for the sorption of methylene blue and 136.98 mg g^{-1} for mercury ions Hg^{2+}. After modification of the SDS surface of Zeolite NaX, the sorption capacity increased to 13.48 mg g^{-1}, and after modification of Zeolite NaX with Ag^0 nanoparticles, the sorption capacity increased to 285.71 mg g^{-1}. These results highlight the potential of the synthesis method for producing synthetic and modified zeolites from rice husks, which can be used to solve various environmental problems, such as purification from dyes and toxic metals. This study serves as an additional method of using waste from rice production since the use of this raw material is limited in Kazakhstan. Additional research can identify new applications and improve the synthesis process to increase efficiency and minimize environmental impacts.

Acknowledgments

This research has been funded by the Science Committee of the Ministry of Science and Higher Education of the Republic of Kazakhstan (Grants No. AP14869646 and BR24992833).

Conflict of Interest

There is no conflict of interest.

Supporting Information

Not applicable.

References

[1] K. S. Obayomi, M. Auta, Development of microporous activated Aloji clay for adsorption of lead (II) ions from aqueous solution, *Heliyon*, 2019, **5**, e02799, doi: 10.1016/j.heliyon.2019.e02799.

[2] E. Koohzad, D. Jafari, H. Esmaeili, Adsorption of lead and arsenic ions from aqueous solution by activated carbon prepared from tamarix leaves, *ChemistrySelect*, 2019, **4**, 12356-12367, doi: 10.1002/slct.201903167.

[3] K. Mirzaei, A. Mohammadi, E. Jafarpour, A. Shojaei, A. L. Moghaddam, Improved adsorption performance of ZIF-8 towards methylene blue dye by hybridization with nanodiamond, *Journal of Water Process Engineering*, 2022, **50**, 103254, doi: 10.1016/j.jwpe.2022.103254.

[4] A. Abutaleb, M. Imran, N. Zouli, A. H. Khan, S. Hussain, M. A. Ali, O. Bakather, M. A. Gondal, N. A. Khan, H. Panchal, S. Zahmatkesh, Fe_3O_4-multiwalled carbon nanotubes-bentonite as adsorbent for removal of methylene blue from aqueous solutions, *Chemosphere*, 2023, **316**, 137824, doi: 10.1016/j.chemosphere.2023.137824.

[5] P. O. Oladoye, T. O. Ajiboye, E. O. Omotola, O. J. Oyewola, Methylene blue dye: Toxicity and potential elimination technology from wastewater, *Results in Engineering*, 2022, **16**, 100678, doi: 10.1016/j.rineng.2022.100678.

[6] M. Eltarahony, E. El-Fakharany, M. Abu-Serie, M. ElKady, A. Ibrahim, Statistical modeling of methylene blue degradation by yeast-bacteria consortium; optimization via agro-industrial waste, immobilization and application in real effluents, *Microbial Cell Factories*, 2021, **20**, 234, doi: 10.1186/s12934-021-01730-z.

[7] M. D. Yahya, H. Abubakar, K. S. Obayomi, Y. A. Iyaka, B. Suleiman, Simultaneous and continuous biosorption of Cr and Cu (II) ions from industrial tannery effluent using almond shell in a fixed bed column, *Results in Engineering*, 2020, **6**, 100113, doi: 10.1016/j.rineng.2020.100113.

[8] B. E. Tokula, A. O. Dada, A. A. Inyinbor, K. S. Obayomi, O. S. Bello, U. Pal, Agro-waste based adsorbents as sustainable materials for effective adsorption of Bisphenol A from the environment: a review, *Journal of Cleaner Production*, 2023, **388**, 135819, doi: 10.1016/j.jclepro.2022.135819.

[9] X. Tian, J. Sarkis, Y. Geng, Y. Qian, C. Gao, R. Bleischwitz, Y. Xu, Evolution of China's water footprint and virtual water trade: a global trade assessment, *Environment International*, 2018, **121**, 178-188, doi: 10.1016/j.envint.2018.09.011.

[10] X. Feng, Q. Liu, L. Yin, B. Fu, Y. Chen, Linking water research with the sustainability of the human–natural system, *Current Opinion in Environmental Sustainability*, 2018, **33**, 99-103, doi: 10.1016/j.cosust.2018.05.012.

[11] F. Nemati, D. Jafari, H. Esmaeili, Highly efficient removal of toxic ions by the activated carbon derived from Citrus limontree leaves, *Carbon Letters*, 2021, **31**, 509-521, doi: 10.1007/s42823-020-00181-7.

[12] E. Aboli, D. Jafari, H. Esmaeili, Heavy metal ions (lead, cobalt, and nickel) biosorption from aqueous solution onto activated carbon prepared from Citrus limetta leaves, *Carbon Letters*, 2020, **30**, 683-698, doi: 10.1007/s42823-020-00141-1.

[13] S. Yu, H. Pang, S. Huang, H. Tang, S. Wang, M. Qiu, Z. Chen, H. Yang, G. Song, D. Fu, B. Hu, X. Wang, Recent advances in metal-organic framework membranes for water treatment: a review, *Science of the Total Environment*, 2021, **800**, 149662, doi: 10.1016/j.scitotenv.2021.149662.

[14] R. Gajera, R. V. Patel, A. Yadav, P. K. Labhasetwar, Adsorption of cationic and anionic dyes on photocatalytic flyash/TiO_2 modified chitosan biopolymer composite, *Journal of Water Process Engineering*, 2022, **49**, 102993, doi: 10.1016/j.jwpe.2022.102993.

[15] I. Chouaybi, H. Ouassif, M. Bettach, E. M. Moujahid, Fast and high removal of acid red 97 dye from aqueous solution by adsorption onto a synthetic hydrocalumite: structural characterization and retention mechanisms, *Inorganic Chemistry Communications*, 2022, **146**, 110169, doi: 10.1016/j.inoche.2022.110169.

[16] H. J. Biswal, A. Yadav, P. R. Vundavilli, A. Gupta, High aspect ZnO nanorod growth over electrodeposited tubes for photocatalytic degradation of EtBr dye, *RSC Advances*, 2021, **11**, 1623-1634, doi: 10.1039/d0ra08124h.

[17] Y. Shi, Q. Chang, T. Zhang, G. Song, Y. Sun, G. Ding, A review on selective dye adsorption by different mechanisms, *Journal of Environmental Chemical Engineering*, 2022, **10**,

108639, doi: 10.1016/j.jece.2022.108639.
[18] Q. Li, Q. Huang, X. Y. Pan, H. Yu, Z. T. Zhao, Adsorption behavior of Cr(VI) by biomass-based adsorbent functionalized with deep eutectic solvents (DESs), *BMC Chemistry*, 2022, **16**, 41, doi: 10.1186/s13065-022-00834-w.
[19] N. C. Thanh, S. Shanmugam, S. Shanmugasundaram, M. S AlSalhi, S. Devanesan, R. Shanmuganathan, N. T. Lan Chi, Comparison of Simarouba glauca seed shell carbons for enhanced direct red 12B dye adsorption: Adsorption isotherm and kinetic studies, *Food and Chemical Toxicology*, 2022, **168**, 113326, doi: 10.1016/j.fct.2022.113326.
[20] L. Sellaoui, M. Bouzidi, D. S. P. Franco, A. S. Alshammari, M. Gandouzi, J. Georgin, N. B. H. Mohamed, A. Erto, M. Badawi, Exploitation of Bauhinia forficata residual fruit powder for the adsorption of cationic dyes, *Chemical Engineering Journal*, 2023, **456**, 141033, doi: 10.1016/j.cej.2022.141033.
[21] K. S. Obayomi, S. Y. Lau, M. Danquah, T. Chiong, M. Takeo, Advances in graphene oxide based nanobiocatalytic technology for wastewater treatment, *Environmental Nanotechnology, Monitoring & Management*, 2022, **17**, 100647, doi: 10.1016/j.enmm.2022.100647.
[22] Z. Chen, Y. Pan, P. Cai, Sugarcane cellulose-based composite hydrogel enhanced by g-C_3N_4 nanosheet for selective removal of organic dyes from water, *International Journal of Biological Macromolecules*, 2022, **205**, 37-48, doi: 10.1016/j.ijbiomac.2022.02.035.
[23] R. M. Mohamed, I. A. Mkhalid, M. A. Barakat, Rice husk ash as a renewable source for the production of zeolite NaY and its characterization, *Arabian Journal of Chemistry*, 2015, **8**, 48-53, doi: 10.1016/j.arabjc.2012.12.013.
[24] D. Dhaneswara, J. Fajar Fatriansyah, M. Bachtiar Yusuf, M. Hanif Abdurrahman, F. Riski Kuskendrianto, Study of Si surface adsorption towards hydrogen molecule, *IOP Conference Series: Materials Science and Engineering*, 2019, **547**, 012038, doi: 10.1088/1757-899x/547/1/012038.
[25] S. Azat, A. V. Korobeinyk, K. Moustakas, V. J. Inglezakis, Sustainable production of pure silica from rice husk waste in Kazakhstan, *Journal of Cleaner Production*, 2019, **217**, 352-359, doi: 10.1016/j.jclepro.2019.01.142.
[26] I. J. Fernandes, C. A. M. Moraes, J. R. J. Egea, V. C. Sousa, Production and characterization of silica materials from rice husk ash by different combustion processes, *Powder Technology*, 2024, **436**, 119473, doi: 10.1016/j.powtec.2024.119473.
[27] C. Santasnachok, W. Kurniawan, H. Hinode, The use of synthesized zeolites from power plant rice husk ash obtained from Thailand as adsorbent for cadmium contamination removal from zinc mining, *Journal of Environmental Chemical Engineering*, 2015, **3**, 2115-2126, doi: 10.1016/j.jece.2015.07.016.
[28] M. Suleimenova, S. Zharylkan, M. Mekenova, A. Mutushev, S. Azat, A. Tolepova, A. Baimenov, A. Satayeva, Z. Tauanov, Fusion-assisted hydrothermal synthesis of technogenic-waste-derived zeolites and nanocomposites: synthesis, characterization, and mercury (II) adsorption, *International Journal of Molecular Sciences*, 2023, **24**, 11317, doi: 10.3390/ijms241411317.
[29] X. Jin, M.-Q. Jiang, X.-Q. Shan, Z.-G. Pei, Z. Chen, Adsorption of methylene blue and orange II onto unmodified and surfactant-modified zeolite, *Journal of Colloid and Interface Science*, 2008, **328**, 243-247, doi: 10.1016/j.jcis.2008.08.066.
[30] M. Kawsar, M. S. Hossain, N. M. Bahadur, S. Ahmed, Synthesis of nano-crystallite hydroxyapatites in different media and a comparative study for estimation of crystallite size using Scherrer method, Halder-Wagner method size-strain plot, and Williamson-Hall model, *Heliyon*, 2024, **10**, e25347, doi: 10.1016/j.heliyon.2024.e25347.
[31] M. Pashai Gatabi, H. Milani Moghaddam, M. Ghorbani, Point of zero charge of maghemite decorated multiwalled carbon nanotubes fabricated by chemical precipitation method, *Journal of Molecular Liquids*, 2016, **216**, 117-125, doi: 10.1016/j.molliq.2015.12.087.
[32] F. K. Mostafapour, M. Yilmaz, A. H. Mahvi, A. Younesi, F. Ganji, D. Balarak, Adsorptive removal of tetracycline from aqueous solution by surfactant-modified zeolite: equilibrium, kinetics and thermodynamics, *Desalination and Water Treatment*, 2022, **247**, 216-228, doi: 10.5004/dwt.2022.27943.
[33] Z. Tauanov, J. Lee, V. J. Inglezakis, Mercury reduction and chemisorption on the surface of synthetic zeolite silver nanocomposites: equilibrium studies and mechanisms, *Journal of Molecular Liquids*, 2020, **305**, 112825, doi: 10.1016/j.molliq.2020.112825.
[34] D. Balarak, M. Baniasadi, S.-M. Lee, M. J. Shim, Ciprofloxacin adsorption onto Azolla filiculoides activated carbon from aqueous solutions, *Desalination and Water Treatment*, 2021, **218**, 444-453, doi: 10.5004/dwt.2021.26986.
[35] J. A. Raj, J. Mathiyarasu, C. Vedhi, P. Manisankar, Electrochemical synthesis of nanosize polyaniline from aqueous surfactant solutions, *Materials Letters*, 2010, **64**, 895-897, doi: 10.1016/j.matlet.2010.01.019.
[36] M. Mudasir, K. Karelius, N. H. Aprilita, E. T. Wahyuni, Adsorption of mercury(II) on dithizone-immobilized natural zeolite, *Journal of Environmental Chemical Engineering*, 2016, **4**, 1839-1849, doi: 10.1016/j.jece.2016.03.016.
[37] A. Bahiraei, J. Behin, Sonochemical immobilization of MnO_2 nanoparticles on NaP-zeolite for enhanced Hg (II) adsorption from water, *Journal of Environmental Chemical Engineering*, 2020, **8**, 103790, doi: 10.1016/j.jece.2020.103790.
[38] G. M. Lüle Şenöz, Removal of basic dyes from wastewater by using natural zeolite: kinetic and equilibrium studies, *NWSA Academic Journals*, 2017, **12**, 130-139, doi: 10.12739/nwsa.2017.12.3.2a0120.
[39] X. Jin, M.-Q. Jiang, X.-Q. Shan, Z.-G. Pei, Z. Chen, Adsorption of methylene blue and orange II onto unmodified and surfactant-modified zeolite, *Journal of Colloid and Interface Science*, 2008, **328**, 243-247, doi: 10.1016/j.jcis.2008.08.066.
[40] C. Wang, J. Yu, K. Feng, L. Wang, J. Huang, Synthesis of porous magnetic zeolite-based material and its performance on removal of Cd^{2+} ion and methylene blue from aqueous solution, *Microporous and Mesoporous Materials*, 2022, **345**, 112256, doi: 10.1016/j.micromeso.2022.112256.

[41] V. J. Inglezakis, S. Azat, Z. Tauanov, S. V. Mikhalovsky, Functionalization of biosourced silica and surface reactions with mercury in aqueous solutions, *Chemical Engineering Journal*, 2021, **423**, 129745, doi: 10.1016/j.cej.2021.129745.
[42] Z. Tauanov, P. E. Tsakiridis, D. Shah, V. J. Inglezakis, Synthetic sodalite doped with silver nanoparticles: characterization and mercury (II) removal from aqueous solutions, *Journal of Environmental Science and Health*, *Part A*, 2019, **54**, 951-959, doi: 10.1080/10934529.2019.1611129.